ORIGINAL ARTICLE

A new pyridazinone exhibits potent cytotoxicity on human cancer cells via apoptosis and poly-ubiquitinated protein accumulation

**Denisse A. Gutierrez · Rebecca E. DeJesus · Lisett Contreras ·
Isela A. Rodriguez-Palomares · Paulina J. Villanueva · Karol S. Balderrama ·
Lenore Monterroza · Manuel Larragoity · Armando Varela-Ramirez ·
Renato J. Aguilera** (ORCID)

Abstract In the last 15 years, pyridazinone derivatives have acquired extensive attention due to their widespread biological activities and pharmacological applications. Pyridazinones are well known for their antimicrobial, anti-viral, anti-inflammatory, anti-cancer, and cardiovascular activities, among others. In this study, we evaluated the anti-cancer activity of a new pyridazinone derivative and propose it as a potential anti-neoplastic agent in acute promyelocytic leukemia cells. Pyr-1 cytotoxicity was assessed on several human cancer and two non-cancerous cell lines by the DNS assay. Pyr-1 demonstrated potent cytotoxicity against 22 human cancer cell lines, exhibiting the most favorable selective cytotoxicity on leukemia (CEM and HL-60), breast (MDA-MB-231 and MDA-MB-468), and lung (A-549) cancer cell lines, when compared with non-cancerous breast epithelial MCF-10A cells. Analyses of apoptosis/necrosis pathways, reactive oxygen species (ROS) production, mitochondria health, caspase-3 activation, and cell cycle profile were performed via flow cytometry. Both *hmox-1* RNA and protein expression levels were evaluated by quantitative real-time PCR and Western blotting assays, respectively. Pyr-1 induced apoptosis in acute promyelocytic leukemia cells as confirmed by phosphatidylserine externalization, mitochondrial depolarization, caspase-3 activation, DNA fragmentation, and disrupted cell cycle progression. Additionally, it was determined that Pyr-1 generates oxidative and proteotoxic stress by provoking the accumulation of ROS, resulting in the overexpression of the stress-related *hmox-1* mRNA transcripts and protein and a marked increase in poly-ubiquitinated proteins. Our data demonstrate that Pyr-1 induces cell death via the intrinsic apoptosis pathway by accumulating ROS and by impairing proteasome activity.

Abbreviations

AL	amyloidosis: immunoglobulin light chain amyloidosis
CC_{25}	Concentration that results in 25% cytotoxicity
CC_{50}	Concentration that results in 50% cytotoxicity
Carboxy-H2DCFDA	6-carboxy-2′,7′-dichlorodihydrofluorescein diacetate
CAD	Caspase-activated DNase
DAPI	4′,6-diamidino-2-phenylindole
DNS	Differential nuclear staining

D. A. Gutierrez · R. E. DeJesus · L. Contreras ·
I. A. Rodriguez-Palomares · P. J. Villanueva ·
K. S. Balderrama · L. Monterroza · M. Larragoity ·
A. Varela-Ramirez · R. J. Aguilera (✉)
The Cytometry, Screening, and Imaging Core Facility, Border
Biomedical Research Center, Department of Biological Sciences,
The University of Texas at El Paso, 500 West University Avenue,
El Paso, TX 79968-0519, USA
e-mail: raguilera@utep.edu

DMSO	Dimethyl sulfoxide
FITC	Fluorescein isothiocyanate
GI$_{50}$	Concentration that results in 50% of cell growth inhibition
H$_2$O$_2$	Hydrogen peroxide
Hmox-1	Heme oxygenase 1
IAP	Inhibitor of apoptosis proteins
IC$_{50}$	concentration that results in 50% of cell growth inhibition
JC-1 reagent	5′,6,6′-tetrachloro-1,1′,3,3′-tetraethylbenzimidazolylcarbocyanine iodide
LC$_{50}$	Lethal concentration that results in 50% of cell death
MM	Multiple myeloma
MTT	3-(4,5-dimethylthiazol-2-yl)-2,5-diphenyltetrazolium bromide
NIM	Nuclear isolation medium
Noxa	protein form of the PMAIP1 gene
PARAs	Pro-apoptotic receptor agonists
PARP-1	Poly [ADP-ribose] polymerase 1
PBS	Phosphate buffer saline
PEG	Polyethylene glycol
PI	Propidium Iodide
PMAIP1	Phorbol-12-myristate-13-acetate-induced protein 1
PS	Phosphatidylserine
Pyr-1	4,5-dichloro-2-[4-chloro-3-(trifluoromethyl)phenyl]-3(2H)-pyridazinone
ROS	Reactive oxygen species
SCI	Selective cytotoxicity index
SRB	Sulforhodamine B

Introduction

According to the World Health Organization (WHO), in 2015, cancer was responsible for 8.8 million deaths globally, being the second leading cause of death worldwide (WHO 2018). The primary cause of death was lung cancer followed by liver, colorectal, stomach, and breast cancer (WHO 2018). In the USA, approximately 41% of men and 38% of women will be diagnosed with cancer during their lifetime (American Cancer Society 2017). Major risk factors include tobacco and alcohol use, unhealthy diet, physical inactivity, and excess body weight (American Cancer Society 2017; WHO 2018). Diverse modalities have emerged to treat cancer patients, such as surgery, radiotherapy, chemotherapy, hormone therapy, targeted and immune therapy, as well as a new developing class of gene therapy (Nastiuk and Krolewski 2016; Ramaswami et al. 2013). Although in recent years, new cancer therapies have emerged, chemotherapy is still the standard treatment for most cancers. Unfortunately, many challenges persist in cancer chemotherapy, mainly on overcoming the highly toxic side effects of many drugs and the eventual appearance of drug-resistant cancers (Al-Lazikani et al. 2012; Hanahan and Weinberg 2000; Hanahan and Weinberg 2011; Nastiuk and Krolewski 2016; Ramaswami et al. 2013). Therefore, the demand for new anticancer drugs is of high importance.

A peculiar attribute of cancer cells is their ability to escape cell death, mainly by upregulating anti-apoptotic proteins (Fulda and Debatin 2006). Many of the anticancer drugs currently used in clinics induce apoptosis indirectly through protein modulation to ultimately activate the apoptotic machinery (Bates and Lewis 2006). Currently, an extensive number of agents continue to be developed to actively regulate this pathway, such as the pro-apoptotic receptor agonists (PARAs) that target the apoptotic extrinsic pathway death receptors, the anti-apoptotic Bcl-2 protein inhibitors, and the apoptotic protein inhibitors (IAP), which serve as endogenous inhibitors of programmed cell death (Bates and Lewis 2006; Tewari and Dhaneshwar 2012).

On the other hand, protein degradation alterations via the ubiquitin-proteasome system are also seen in diverse human diseases, including cancer (Dou and Zonder 2014; Naujokat and Hoffmann 2002; Zhang et al. 2013). An increase in proteasome activity has been previously associated with malignant diseases and cancer progression (Chen et al. 2017; Loda et al. 1997). On the contrary, proteasome inhibition has been shown to induce tumor cell growth suppression and apoptosis, as a result of pro- and anti-apoptotic protein imbalances (Dou and Zonder 2014; Li and Dou 2000). Furthermore, in the last 15 years, proteasome inhibition arose as a novel cancer therapeutic approach. In 2003, bortezomib emerged as the first FDA-approved proteasome inhibitor for multiple myeloma (MM) treatment; attaining a 2–3-fold positive survival rate (Dou and Zonder 2014; Zhang et al. 2013). Due to the success of bortezomib treatment for MM patients, it was later used for AL

amyloidosis (Reece et al. 2011) and in combination with other drugs for the treatment of non-Hodgkin lymphoma (Leonard et al. 2006). However, not all cancer patients responded to bortezomib therapy, especially those with solid tumors, which are often resistant to this drug (Dou and Zonder 2014). To overcome the limitations of bortezomib therapy, second-generation proteasome inhibitors have been developed, mainly to increase anti-tumor efficacy and to reduce toxicity (Dou and Zonder 2014; Contreras et al. 2018).

Recently, pyridazinone derivatives have received substantial attention due to their extensive biological activities. For example, they have been described as anti-inflammatory (Mogilski et al. 2015; Saini et al. 2016), analgesic (Mogilski et al. 2015), anti-viral (Wang et al. 2015), anti-parasitic (Jacomini et al. 2016), anti-microbial (Faidallah et al. 2013), anti-diabetic (Rathish et al. 2009), anti-cancer (Jin et al. 2015; Zhou et al. 2014), anti-tubercular (Li et al. 2014), as protein kinase inhibitors (Dorsch et al. 2015; Elagawany et al. 2013; Liu et al. 2016), and have also been shown to affect the cardiovascular system (Asif 2015; Costas et al. 2015), among others.

A high throughput drug screening project to uncover novel anti-cancer drugs was initiated that led to the testing of 4640 chemical compounds from the ChemBridge DIVERSet chemical library on the acute lymphoblastic lymphoma cell line CEM and the triple-negative breast cancer cell line MDA-MB-231. This screening project identified six pyridazinone derivatives as potential anticancer agents (see Fig. 1). Out of these six pyridazinones, Pyr-1 was found to be the most potent drug against the human cancer cell lines that were tested. Due to these findings, our work focused on Pyr-1 (pyridazinone derivative, 4,5-dichloro-2-[4-chloro-3-(trifluoromethyl)phenyl]-3(2H)-pyridazinone) as a potent apoptotic inducer on acute promyelocytic leukemia HL-60 cells. Additionally, it was demonstrated that Pyr-1 was also cytotoxic to 22 additional human cancer cell lines, displaying CC_{50}'s at the low micromolar or nanomolar levels. Pyr-1 treatment also leads to stress-related events that included the accumulation of ROS, poly-ubiquitinated proteins, as well as the overexpression of *hmox-1* gene and protein. Based on the aforementioned results, we propose Pyr-1 as a new potent anti-cancer agent that may result in the development of new anti-tumor therapies.

Materials and methods

Cell lines and culture conditions

Lymphoma/leukemia (CEM, HL-60, RAMOS, and MT2), B lymphoblastic myeloma (RPMI-8226 and U266), lung cancer (NCI-H358, NCI-H460, and A-549), ovarian carcinomas (OVCAR-3, 5, and 8), as well as breast carcinoma (HCC1419) cell lines were cultured in RPMI-1640 medium (Hyclone, Logan UT) supplemented with 100 U/mL of penicillin and 100 μg/mL of streptomycin (Lonza, Walkersville, MD). Additionally, 10% fetal bovine serum (FBS; Hyclone) was added to all the previously mentioned cell lines, except for HL-60 and OVCAR-3, which were grown in 20% of FBS. The MDA-MB-231, MDA-MB-231 LM2-4, MDA-MB-468, MCF-7, PANC-1, LNCaP, A375, and Hs-27 cell lines were grown in DMEM medium (Hyclone) supplemented with 10% FBS (Hyclone) and 100 U/mL of penicillin and 100 μg/mL of streptomycin (Lonza). Also, 10 μg/mL of insulin was added to the MCF-7 cell line. OV-90 cells were cultured in 50% of MCDB 105 medium (Sigma, M6395) and 50% of Gibco medium 199 (Gibco, 11150-59), supplemented with 15% FBS, 100 U/mL of penicillin, and 100 μg/mL of streptomycin. Lastly, PC-3 and MCF10A cells were grown in DMEM F/12 media containing 10% FBS, 100 U/mL of penicillin and 100 μg/mL of streptomycin. Furthermore, 20 ng/mL of epidermal growth factor (EGF), 0.5 μg/mL of hydrocortisone, and 10 μg/mL of insulin were added to the MCF10A cell line. All previously mentioned cell types were consistently incubated at 37 °C in a humidified with 5% CO_2 atmosphere.

Differential nuclear staining assay

To examine the potential cytotoxicity of Pyr-1, the DNS assay was used, which is a validated high throughput screening method to identify cytotoxic compounds (Lema et al. 2011). The DNS assay consists of labeling the cells with two different nucleic acid fluorescent dyes: Hoechst (Invitrogen, Eugene, OR, USA) and Propidium Iodide (PI; MP Biomedicals, Solon, OH, USA). Hoechst permeates and stains the nuclei of healthy and dead cells, whereas PI permeates only the cells with compromised membranes, defined as dead cells, to subsequently stain their nuclei (Lema et al. 2011). In this assay, Hoechst (blue) dye labels the total number of cells in the captured images, whereas cells
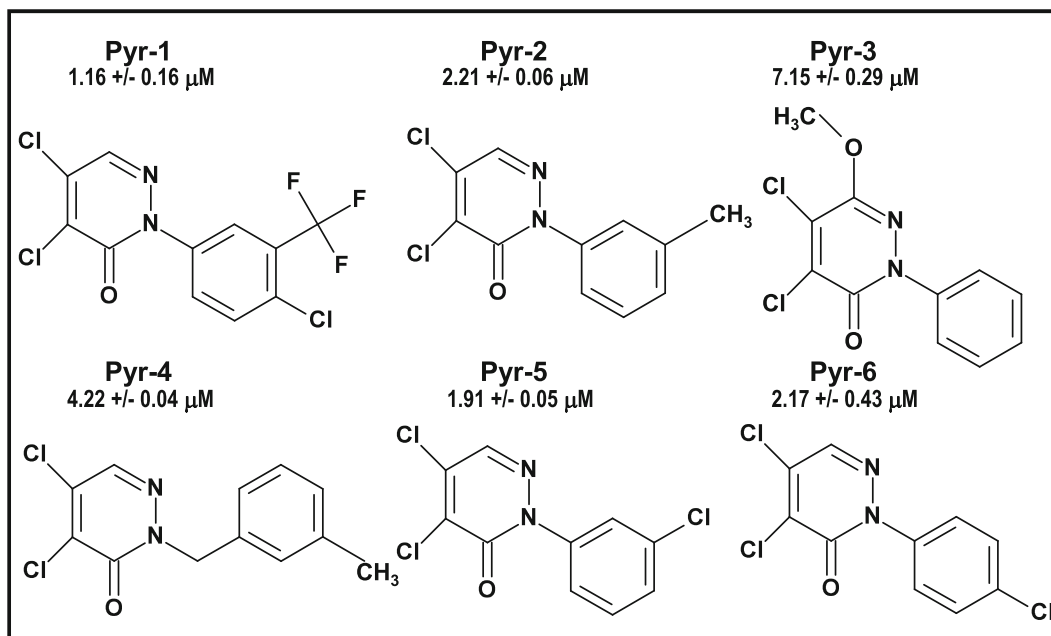
Fig. 1 The structures and CC_{50}'s of the six most cytotoxic pyridazinone compounds on MDA-MB-231 cells identified from a primary and secondary screening of 4640 chemical compounds. The identified pyridazinones were named Pyr-1 to -6 and are indicated in the figure. The Pyr-1 CC_{50} values when tested in MDA-MB-231 cells after 48 h of exposure are shown below each compound name in micromolar (μM). Pyr-1 was the most cytotoxic with a CC_{50} value of 1.16 μM

that are positive for both dyes, Hoechst and PI (red) signal colocalization, are recognized and defined as the dead cell population (Lema et al. 2011). Prior to each assay, cell viability was analyzed to ensure that cells were at least 95% viable using PI staining and the Gallios flow cytometer (Beckman Coulter, Miami, FL). Cells were seeded in 96-well microplates at a density of 10,000 cells per well in 100 μL of media and incubated overnight. A concentration gradient of Pyr-1 from 5 to 0.1 μM was tested. The following controls were included in each experiment: vehicle (1% v/v DMSO), positive for death (1 mM H_2O_2), and untreated cells. Each experimental point, as well as the controls, was assessed in triplicate. Additionally, two incubation times were performed, 48 and 72 h. Two hours prior the end of the incubation period, a mixture of the two fluorescent dyes (1 μg/mL final concentration) were added to each well, and plates were incubated for the remaining 2 h. Thereafter, image acquisition was implemented using the IN Cell Analyzer 2000 system (GE Healthcare, Pittsburg PA, USA). Four contiguous images were acquired per well creating 2 × 2 montages by using a 10× objective and from two individual fluorescent channels (Hoechst and PI emission signals)

accordingly. Captured images were segmented and analyzed for both living and dead cells using the IN Cell Analyzer Workstation 3.2 software (GE Healthcare), obtaining the percentages for each cell subpopulation and from each individual well.

Cytotoxic concentration 50% and selective cytotoxicity index values

The CC_{50} was defined as the Pyr-1 concentration needed to kill 50% of the cell population. The percentage of dead cells obtained from the vehicle control (DMSO) was subtracted from each individual experimental point to eliminate the background of dead cells, and then, the resulting values were used to calculate the CC_{50}. Next, a linear interpolation equation was used to determine the CC_{50} values (Varela-Ramirez et al. 2011). Due to the shortened compound exposure period and to detect a dose-response, cells were exposed to the CC_{50} and twice that concentration of Pyr-1 (2× CC_{50}). A selective cytotoxicity index (SCI) denotes the capacity of an experimental compound to preferentially kill cancer cells, causing less or insignificant damage to non-cancerous cells. The SCI Pyr-1 values were calculated by dividing

the CC_{50} of the non-cancerous control cell line by the CC_{50} of the cancer cell line as previously detailed (Robles-Escajeda et al. 2016).

Reactive oxygen species detection assay

Analysis of ROS production in Pyr-1-treated cells was conducted via carboxy-H_2 DCFDA (6-carboxy-2′,7′-dichlorodihydrofluorescein diacetate) fluorescein reagent (Invitrogen, C400) and monitored via flow cytometry (Eruslanov and Kusmartsev 2010; Invitrogen 2006). The carboxy-H_2 DCFDA indicator, which is initially a non-fluorescent and cell permeable reagent, is transformed intracellularly into its green fluorescent form (carboxydichlorofluorescein) by esterases when oxidation occurs. HL-60 cells were seeded in 24-well plates at a concentration of 100,000 cells per well and incubated at optimal conditions overnight. Pyr-1 and control treatments were applied to the cells and they were incubated for 18 h to let the oxidation process occur. Bortezomib (60 nM) and H_2O_2 (100 μM) were incorporated as positive controls as well as untreated and 1% DMSO vehicle controls. Treated cells were collected in flow cytometer tubes and centrifuged for 5 min at 262g to remove treatments. Cell pellets were re-suspended in pre-warmed PBS containing the carboxy-H_2 DCFDA probe to provide a final concentration of 10 μM (loading buffer). Cells were placed back at optimal conditions (37 °C, 5% CO_2) for 1 h. To remove the loading buffer, cell suspensions were spun down (5 min, 262g) and re-suspended in 500 μL of PBS. Cells were subsequently analyzed through the Gallios flow cytometer (Beckman Coulter), acquiring 10,000 cell events per sample and analyzed via Kaluza software (Beckman Coulter).

Mitochondrial membrane integrity via JC-1 assay

Examination of mitochondrial membrane integrity after exposure to Pyr-1 was accomplished by means of the MitoProbe JC-1 assay kit (Molecular Probes, M34152) and flow cytometry. HL-60 cells seeded in 24-well plates at a density of 100,000 cells in 1 mL of cell culture media per well were treated with Pyr-1 and controls (as above mentioned) in triplicate for 5 h. Cells were then collected and centrifuged at 262g for 5 min. A total of 500 μL of PBS containing 5 μL (2 μM final concentration) of JC-1 reagent (5′,6,6′-tetrachloro-1,1′,3,3′-tetraethylbenzimidazolylcar-bocyanine iodide)

was used to re-suspend the cell pellets, and then, they were incubated at 37 °C, 5% CO_2 for 30 min. Cells were washed once with pre-warmed PBS after incubation and were immediately examined by flow cytometry. Approximately 10,000 cells/events were acquired per sample and data analysis was achieved by the CXP software (Beckman Coulter).

Analysis of apoptosis/necrosis by annexin V-FITC/PI assay

To investigate the mechanism of cell death induction by Pyr-1, the annexin V-FITC Kit was employed (Beckman Coulter, Miami, FL, USA). HL-60 cells were seeded in 24-well plates at a concentration of 100,000 cells per well containing 1 mL of culture media and incubated at 37 °C, 5% CO_2 overnight. Treatments were applied to cells in triplicate and plates were incubated at optimal conditions for 24 h. Solvent (1% DMSO), untreated, and (1 mM) H_2O_2 positive controls were included. Cells were harvested in flow cytometry tubes and centrifuged for 5 min at 262g. Cell pellets were re-suspended in 103.5 μL of the following mixture: 100 μL of the 1× binding buffer, 1 μL annexin V-FITC, and 2.5 μL of propidium iodide. Cells were gently re-suspended to facilitate the exposure of the fluorophores to the cells and kept on ice for 30 min in the dark. Subsequently, 300 μL of ice-cold PBS was added to each tube and immediately analyzed via flow cytometry (Cytomics FC 500, Beckman Coulter). Nearly 10,000 events (cells) per sample were collected, and the CXP software (Beckman Coulter) was utilized for data analysis.

Caspase-3 assay

Caspase-3 activation was analyzed by using a NucView 488 caspase-3 substrate assay kit (Biotium, Hayward, CA). The principle of this assay consists of a fluorogenic substrate which is cleaved by an active caspase-3 releasing a product that after binding to the DNA emits a bright green fluorescence signal. HL-60 cells were plated in 24-well plates (100,000) and exposed to Pyr-1 for 6 h. Controls were included as previously described. After the incubation period, cells were harvested in flow cytometry tubes and centrifuged at 262g, for 5 min. Cell pellets were disrupted by adding 200 μL of PBS containing 5 μL of NucView 488 Caspase-3 substrate (5 μM final concentration), and cell suspensions were incubated at room temperature for

30 min in the dark. After this step, 300 μL of PBS was added to the cell mixture and immediately analyzed by flow cytometry. Cells emitting a green positive signal were denoted as apoptotic (caspase-3 active). Approximately 10,000 cells (events) were collected per sample and analyzed by using Kaluza Flow Cytometry Software (Beckman Coulter).

Cell cycle analysis

HL-60 cells were seeded in 24-well plates at a concentration of 100,000 cells containing 1 mL of culture media per well. Cells were treated with 0.25 μM (CC_{25}) and 0.39 μM (CC_{50}) of Pyr-1 for a 72-h period. The controls included for this series of experiments were as previously described. Cells were subsequently collected in flow cytometry tubes, centrifuged at 262g for 5 min, and gently re-suspended in 100 μL of fresh culture media. Then, 200 μL of nuclear isolation medium (NIM)-DAPI solution (NPE Systems, Inc. Pembroke Pines, FL, USA and Beckman Coulter) was added to the cell suspension and immediately analyzed via flow cytometry. The NIM-DAPI reagent is able to permeabilize and stain the nuclei of the cells allowing to quantify their DNA content by using an FL-9 detector and the 405-nm laser for excitation purposes (Gallios). This FL-9 detector captures the fluorescence signal emitted when DAPI is intercalated to DNA (461 nm); therefore, omitting the signal when DAPI is complexed with RNA (~ 500 nm). For the purpose of obtaining a well-defined cell cycle distribution profile, 100,000 cells (events) were acquired per sample and analyzed via Kaluza Flow Cytometry Software (Beckman Coulter). Each experimental point, as well as their corresponding controls, were processed concurrently and assessed in triplicate.

Western blot analysis

To evaluate the ability of Pyr-1 to induce accumulation of cellular poly-ubiquitinated proteins, Western blot approach was performed after several times of exposure. Also, the same strategy was used to quantify the expression levels of both *hmox-1* and *noxa* stress-related proteins. Cell lysates were prepared from HL-60 cells (3 × 10^6) treated with Pyr-1, MG132, or bortezomib at different time points. Both MG132 and bortezomib (also known as MG-341) were used interchangeably in these series of experiments as positive controls of proteasome

activity inhibition. After termination of each incubation period, cells were harvested and centrifuged at 262g for 5 min. Cell pellets were washed with 1 mL of PBS and centrifuged again at 1000g for 6 min. Then, the pellets were re-suspended in 50 μL of 2× laemmli buffer (120 mM Tris-HCl, 0.1% β-mercaptoethanol, 4% SDS, 20% glycerol, and 0.02% (v/v) bromophenol blue) and boiled for 10 min at 100 °C. Protein content was quantified utilizing a NanoDrop N-1000 system (Thermo, Fisher Scientific). A total of 100 μg of cell protein extract was separated using a sodium dodecyl sulfate–polyacrylamide gel electrophoresis (SDS-PAGE) gel and transferred onto a polyvinylidene difluoride (PVDF) membrane. Antibodies were acquired from the following sources: α (anti)-ubiquitin mouse monoclonal (1:1000 dilution; Santa Cruz Biotech, Dallas, TX), α-*noxa* mouse monoclonal (1:1000; Thermo Fischer, Waltham, MA), α-*hmox-1* mouse monoclonal (1:200; Santa Cruz Biotech), α-β Actin peroxidase (1:25,000; Sigma Aldrich, St. Louis, MO), and polyclonal goat anti-mouse conjugated to horseradish peroxidase (Thermo Scientific). The Image Studio™ Lite (LI-COR) Software was utilized for densitometry analysis.

Quantitative real-time PCR assay

The quantification of both *hmox-1* and *noxa* (PMAIP1) mRNA transcripts was carried out by real-time PCR protocols. The total RNA was extracted from HL-60 cells (1X10^6) treated with Pyr-1, bortezomib, or the vehicle control, 0.3% v/v PEG-400 for 6 h using the RNeasy Mini kit (Qiagen, 74104). cDNA synthesis was performed by using the RT^2 HT First Strand Kit (Qiagen; 330411). Quantitative real-time PCR was accomplished using the iCycler Thermal Cycler (Bio-Rad, 582BR). A 25-μL reaction was prepared containing 12.5 μL of RT^2 SYBR Green (Qiagen; 330512), 3.5 μL of each forward and reverse primers (5 pmol/μL) ***noxa*** (PMAIP1); forward sequence: *5′ CTCAAACC TCCAAAAGCC 3′*, reverse: *5′ CCTGAGCAGAAGAG TTTGGA 3′*, **hmox-1** forward sequence: 5′ *CTCAAACC TCCAAAAGCC* 3′, reverse: 5′ *TCAAAAACCACCCC AACCC* 3′), 4 μL of cDNA template and 1.5 μL of nuclease-free water. All PCR experiments contained three technical replicates and included a negative control consisting of H_2O, instead of DNA template, and three independent experiments were performed. Fold change numbers were obtained using the comparative C_T method (Schmittgen and Livak 2008). Data were normalized

to a housekeeping gene (GAPDH) for equal loading amounts.

Statistical analysis

The Student's t-test was utilized to calculate P values among sample groups, and P values ≤ 0.05 were considered significant. In most cases, for each data point, an average was calculated from triplicate values with its corresponding standard deviation displayed.

Results

Pyr-1 exerts potent cytotoxic activity against a panel of human cancer cell lines

A Chembridge DIVERSet chemical library was used to screen for drugs potentially toxic to human cancer cells. A primary screening of 4640 compounds was performed in tandem on the MDA-MB-231 and CEM cell lines, out of which six pyridazinones were detected as the most potent compounds (Fig. 1). The CC_{50} values of the six compounds on MDA-MB-231 are shown in Fig. 1, indicating that Pyr-1 was the most potent pyridazinone of those originally detected by our screen. Based on the chemical structures of the six pyridazinone derivatives, the increased toxicity detected with Pyr-1's can be attributed to the trifluoromethyl radical localized at the carbon 3 of the molecule (Fig. 1). The cytotoxic activity of Pyr-1 was examined by the differential nuclear staining (DNS) assay (Lema et al. 2011). Lymphoma/leukemia and myeloma cell lines, which grow in suspension, were incubated for 48 h with Pyr-1. Since the adherent cells generally divide at a slower rate than the non-adherent cell lines, the MDA-MB-231, MDA-MB-231 LM2-4, MDA-MB-468, MCF-7, HCC1419, PANC-1, PC-3, LnCap, A375, OVCAR-8, 5 and 3, OV-90, NCI-H358, NCI-H460, and A-549 adherent cancer cells lines were incubated for 72 h in the presence of Pyr-1. After treatment, images were acquired and analyzed to determine the percentages of live/dead cells and their cytotoxicity (CC_{50} concentrations). The CC_{50} values ranged from 0.33 to 2.63 μM, corresponding to the breast carcinoma MDA-MB-231 and the large cell lung cancer cell line NCI-H460, respectively (Table 1). The MCF-10A non-cancerous human epithelial breast cancer cell line and the Hs-27 human foreskin fibroblast cell line were included and

used for comparison purposes. The CC_{50} values obtained from each individual cancer cell line were compared to the MCF-10A cells and the SCI values ranged from 0.47- to 3.73-fold (Table 2). Furthermore, Pyr-1 exhibited tumor-selective cytotoxicity showing high (more than 3-fold) SCI values on the HL-60 promyelocytic and CEM T lymphoblastic leukemia cell lines of 3.02 and 3.61, respectively. Similar values were determined for the lung carcinoma A-549 cell line (SCI = 3.32), and the triple negative breast adenocarcinoma cell lines; MDA-MB-231 (SCI = 3.73) and MDA-MB-468 (SCI = 3.51; Table 2).

The HL-60 cell line was selected for further experimentation for two reasons. We first investigated whether Pyr-1 acts as a proteasome inhibitor by comparing its activity to two previously reported proteasome inhibitors that were primarily tested in the HL-60 cell line (Contreras et al. 2018). In addition, apoptosis assays on the HL-60 non-adherent cancer cells are easier to process than the adherent MDA-MB-231 cells by flow cytometry as the adherent cells require additional cellular manipulations to process (use of cell scrappers or trypsin).

Pyr-1 induces ROS accumulation to initiate cell death

To further elucidate the mode of action of Pyr-1, we measured reactive oxygen species accumulation in HL-60 cells treated with Pyr-1 for 18 h. After the incubation period, HL-60 cells were stained with 10 μM of the carboxy-H2 DCFDA ROS detection reagent and incubated for an additional 1 h under optimal conditions (see details in "Materials and methods"). As shown in Fig. 2a, the green fluorescent signal was detected as an indication of ROS accumulation by flow cytometry. Bortezomib, a well-known proteasome inhibitor and ROS inducer, was included as a positive control (Fribley et al. 2004; Ling et al. 2003a; Perez-Galan et al. 2006). As shown in Fig. 2a, HL-60 cells generated a significant amount of ROS when exposed to Pyr-1 ($P < 0.001$) or bortezomib ($P < 0.001$) for 18 h. These findings indicate that Pyr-1 disturbs cellular homeostasis by increasing ROS, which can lead to the induction of apoptosis.

Pyr-1 elicits a robust change in mitochondrial transmembrane potential

ROS overproduction can result in damage to DNA, proteins, and lipids (Suski et al. 2018). Also, high ROS levels

Table 1 Cytotoxic concentration 50% (CC_{50}) values of Pyr-1 in different cell lines after 48 and 72 h of exposure

Cell line	Origin	CC_{50} 48 h (μM)[c]
HS-27	Foreskin epithelial	0.36 ± 0.0947[a]
MCF-10A	Breast epithelial	1.48 ± 0.253
CEM	T Lymphoblastic leukemia	0.41 ± 0.049
HL-60	Promyelocytic leukemia	0.49 ± 0.32
RAMOS	Burkitt's lymphoma	2.88 ± 0.339
MT2	T cell leukemia	1.54 ± 0.025
RPMI-8226	B Lymphoblastic myeloma	2.57 ± 0.10
U266	B Lymphoblastic myeloma	0.71 ± 0.00071
Cell line	Origin	CC_{50} 72 h (μM)[a]
HS-27	Foreskin epithelial	1.97 ± 0.066
MCF-10A	Breast epithelial	1.23 ± 0.61
MDA-MB-231	Breast adenocarcinoma	0.33 ± 0.022
MDA-MB-231 LM2-4	Breast metastatic[b]	0.95 ± 0.164
MDA-MB-468	Breast adenocarcinoma	0.35 ± 0.068
MCF-7	Breast adenocarcinoma	1.10 ± 0.25
HCC1419	Breast carcinoma	2.05 ± 0.176
PANC-1	Pancreas carcinoma	2.52 ± 0.27
PC-3	Prostate adenocarcinoma	2.08 ± 0.03
LNCaP	Prostate carcinoma	2.44 ± 0.23
A375	Melanoma	0.78 ± 0.11
OVCAR-8	Ovarian carcinoma	0.67 ± 0.068
OVCAR-5	Ovarian carcinoma	0.45 ± 0.066
OVCAR-3	Ovarian adenocarcinoma	0.64 ± 0.069
OV-90	Ovarian adenocarcinoma (metastatic)	1.9 ± 0.096
NCI-H358	Non-small cell lung cancer	1.75 ± 0.0916
NCI-H460	Large cell lung cancer	2.63 ± 0.028
A-549	Lung carcinoma	0.37 ± 0.029

[a] "±" values refer to standard deviations

[b] This metastatic variant breast cancer cell line was generated by Munoz et al. (2006)

[c] The cytotoxic concentration 50% (CC_{50}) is defined as the concentration of experimental drug needed to kill 50% of the cell population, either after 48 or 72 h of exposure

Table 2 Selective cytotoxicity index (SCI) values from Pyr-1-treated cancer cells after 48 and 72 h of treatment

Cell line	SCI (48 h)[a]
CEM	3.61
HL-60	3.02
RAMOS	0.51
MT2	0.96
RPMI-8226	0.58
U266	2.08
Cell line	SCI (72 h)[a]
MDA-MB-231	3.73
MDA-MB-231 LM2-4	1.29
MDA-MB-468	3.51
MCF-7	1.18
HCC1419	0.60
PANC-1	0.48
PC-3	0.59
LNCaP	0.50
A375	1.58
OVCAR-8	1.84
OVCAR-5	2.73
OVCAR-3	1.92
OV-90	0.65
NCI-H358	0.70
NCI-H460	0.47
A-549	3.32

[a] SCI values were calculated dividing the CC_{50} of the non-cancerous cell line MCF-10A by the CC_{50} of the cancer cell line

we evaluated the mitochondrial membrane potential of Pyr-1-treated HL-60 cells using the JC-1 polychromatic fluorescence reagent. HL-60 cells were incubated with Pyr-1 for 5 h at the CC_{50} and $2\times CC_{50}$ concentrations, 0.39 and 0.78 μM, respectively, and subsequently stained with the JC-1 reagent and examined by flow cytometry as previously described (Santiago-Vazquez et al. 2016). Pyr-1-treated cells showed an increased dose-dependent mitochondrial depolarization that was statistically significant when compared to the solvent ($P < 0.001$) and untreated ($P < 0.001$) controls (Fig. 2b). These results indicate that Pyr-1 mechanism of cell death is through apoptosis via mitochondrial depolarization.

Pyr-1 induces significant phosphatidylserine externalization

To corrobotate whether Pyr-1 utilizes apoptosis to induce cell death, we measured phosphatidylserine (PS)
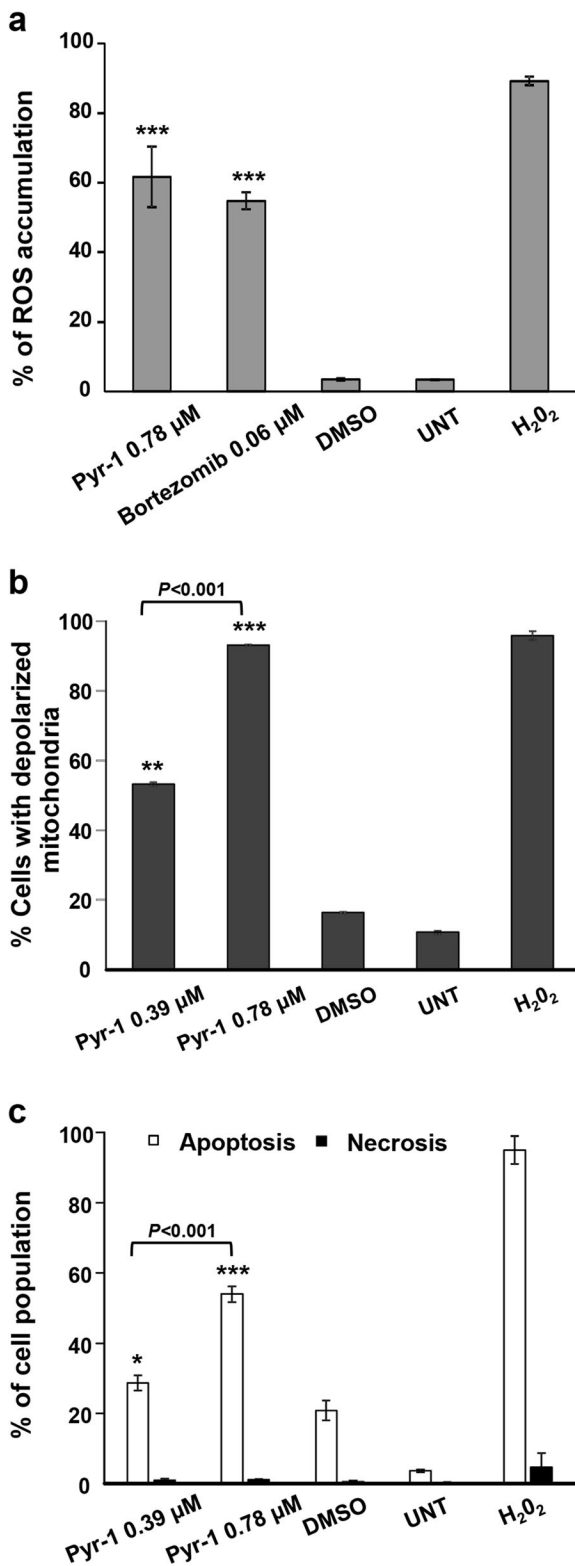
can enhance mitochondrial permeability and elicit mitochondrial membrane depolarization with the widespread destruction of mitochondrial function (Torres-Roca et al. 1995). Moreover, the intrinsic apoptotic pathway is initiated through diverse non-receptor stimuli leading to a loss of mitochondrial transmembrane potential and the release of several pro-apoptotic proteins (Elmore 2007). To further determine the mechanism of cell death induced by Pyr-1,

Fig. 2 Pyr-1 induces significant ROS production, mitochondrial membrane depolarization, and PS externalization in acute promyelocytic leukemia cells. **a** Pyr-1 provokes ROS accumulation after 18 h of exposure to HL-60 cells. H_2O_2 and bortezomib were used as positive controls. Percentages of bars represent the average of three replicates. **b** HL-60 cells treated with Pyr-1 for 5 h exhibited a robust mitochondrial depolarization in a dose-response manner. Cells treated with 0.39 and 0.78 μM of Pyr-1 were examined by flow cytometry after staining with the JC-1 reagent. The green fluorescent signal was detected for cells with depolarized mitochondrial membranes (monomers), whereas a red fluorescent signal was identified for cells with healthy unpolarized membranes (aggregates). Percentages represent averages of three technical replicates. **c** HL-60 cells treated with Pyr-1 exhibited a dose-dependent apoptotic response measured after 24 h of exposure. Cells were treated with Pyr-1 at the CC_{50} (0.39 μM) concentration as well as at 2× CC_{50} (0.78 μM) and analyzed by flow cytometry after staining with annexin V-FITC and PI. Cells either positive for annexin V-FITC and PI or only for annexin V-FITC were annotated as apoptotic cells, the former representing late and the latter representing early apoptosis. Percentages shown in the bar graphs represent the total value of early and late apoptosis (open bars). Cells that were positive only for PI were considered as necrotic (black bars). 1 mM H_2O_2, untreated and vehicle (1% DMSO) controls were included in all assays. Statistical analyses were performed using two-tailed Student's paired t test, and the asterisk annotations in each graph represent statistical significance of the treatments against the vehicle control (DMSO); $*P < 0.05$, $**P < 0.01$, and $***P < 0.001$

externalization in Pyr-1-treated HL-60 cells by using the annexin V-FITC/PI assay (Contreras et al. 2018; Robles-Escajeda et al. 2016). For these experiments, two concentrations of Pyr-1 were used, 0.39 μM (CC_{50}) and 0.78 μM (2× CC50). Our results indicate that Pyr-1 induces significant PS externalization in a dose-response manner, as compared to solvent control; $P < 0.05$ for 0.39 μM and $P < 0.001$ for 0.78 μM of Pyr-1 (Fig. 2c). As expected, the H_2O_2 positive control for death caused the highest percentage of PS externalization (95.1%), whereas DMSO-treated and untreated cells showed low levels of PS externalization of 20.8% and 3.63%, respectively (Fig. 2c). These findings suggest that Pyr-1 induces PS externalization, a biochemical hallmark of apoptosis.

Pyr-1 induces caspase-3 activation

Caspase-3 activation is a critical biochemical occurrence during the execution phase of apoptosis, leading to the cleavage of several target proteins such as PARP-1,

CAD, and many others (Elmore 2007). To further support and extend the findings that suggest that Pyr-1 induces apoptosis, caspase-3 activation was measured in cells exposed to Pyr-1. HL-60 cells were treated with 0.5 μM of Pyr-1 for 8 h and subsequently stained with the NucView caspase-3 substrate and analyzed via flow cytometry (Robles-Escajeda et al. 2013). Pyr-1 treatment in HL-60 cells induced a statistically significant activation of caspase-3 ($P < 0.001$; Fig. 3) when compared to the DMSO control. Interestingly, the percentage of caspase-3 activation on cells exposed to Pyr-1 (84.8%) was similar to that observed in the positive control H_2O_2 (98.6%). These results provide further support that Pyr-1 induces cell death via well-known apoptotic events.

Pyr-1 alters normal cell cycle profile

Cytometric analyses of cell cycle progression were performed to investigate if Pyr-1 can disrupt this process. HL-60 cells were exposed to Pyr-1's CC_{25} (0.25 μM) and CC_{50} (0.39 μM) concentrations and incubated for 72 h to subsequently be treated with a nuclear isolation medium (NIM) containing the DNA-intercalating agent DAPI (Robles-Escajeda et al. 2016). The DAPI fluorescent signal of each treatment was measured to quantify the DNA content in the different samples. The vehicle (solvent), untreated and H_2O_2 control samples were also included concurrently as in the previous assays. As
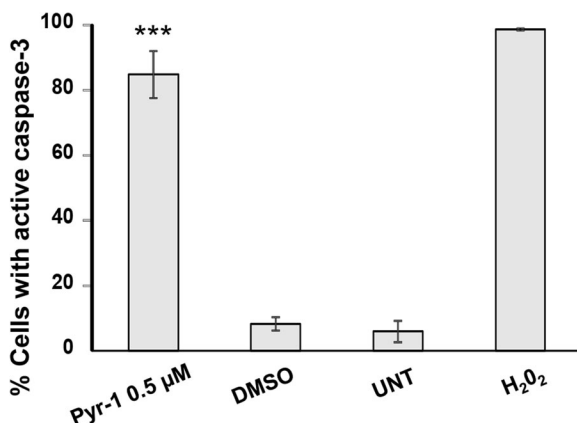

Fig. 3 Flow cytometry analysis revealed that Pyr-1 activates caspase-3 in HL-60 cells. Cells positive for NucView 488, a DNA dye coupled to the caspase-3 recognition sequence, indicated caspase-3 activation. Histograms and percentages of cells with caspase-3 activity shown on bar graph are representative of four replicates. Pyr-1 and DMSO statistical difference of ***$P < 0.001$

expected, an increase of DNA fragmentation was found in cells treated with Pyr-1 which was denoted by an increase of the sub-G0-G1 subpopulation (CC_{25} 25.5% and CC_{50} 47%; Fig. 4a). Interestingly, the G0/G1 and G2/M subpopulations displayed a significant decrease in Pyr-1-treated cells when compared to the solvent control (Fig. 4b, c). In addition, the disruption of the cell cycle observed in Pyr-1-treated cells was similar to the trend observed in the positive control of cell damage (H_2O_2; Fig. 4a–d). Thus, our results indicate that Pyr-1 induced significant increases of apoptosis-induced DNA fragmentation, sub-G0/G1 subpopulations, and altered the cell cycle profile as evidenced by a reduction in the percentages of the G0/G1 and G2/M subpopulation.

Pyr-1 produces a rapid accumulation of poly-ubiquitinated proteins

Some groups have associated the generation of ROS with proteasome inhibition resulting in apoptosis (Brnjic et al. 2014; Fribley et al. 2004; Ling et al. 2003b; Perez-Galan et al. 2006). To further investigate the mechanism by which Pyr-1 induces apoptosis, we examined its ability to inhibit proteasome activity. In the past, it has been observed that accumulation of poly-ubiquitinated proteins is an indication of proteasome impairment (Brnjic et al. 2014; Contreras et al. 2018; D'Arcy et al. 2011; Wada et al. 2015). Therefore, we measured poly-ubiquitinated proteins on HL-60 cells exposed to Pyr-1 at different time points by Western blotting. MG-132, a well-known proteasome inhibitor, was included as a positive control (Guo and Peng 2013). Our results demonstrated an accumulation of poly-ubiquitinated proteins after 1 h of treatment with either Pyr-1 or MG-132. Poly-ubiquitinated protein accumulation was augmented after 3, 5, and 8 h of incubation time for both Pyr-1 and MG132, as presented in Fig. 5a, b. The housekeeping protein β-actin was used as a protein loading control. Densitometry analyses of the ubiquitin antibody response were performed by quantifying its band signal intensity and using the loading control protein for normalization purposes. Data presented in Fig. 5c shows that Pyr-1- and MG132-treatment led to a 3-fold increase in poly-ubiquitinated proteins in the HL-60 cell line. These results suggest that Pyr-1 acts as a proteasome inhibitor in HL-60 cells in a time-dependent manner.
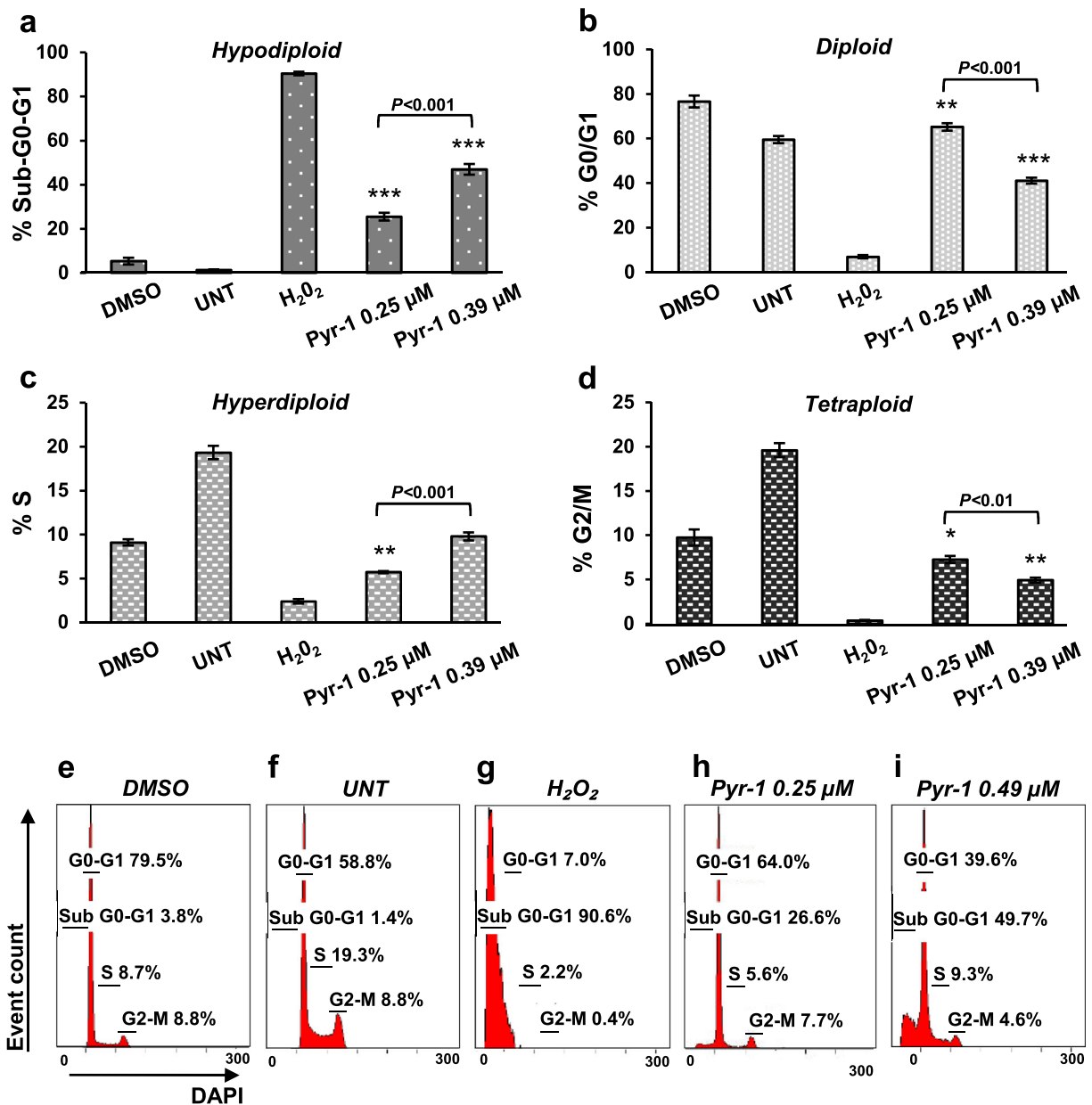
Fig. 4 Analysis of the effects of Pyr-1 treatment on cell cycle progression. Cell cycle progression was evaluated by flow cytometry after 72 h of exposure of HL-60 cells to Pyr-1. The DAPI fluorescent signal was used to quantify the cell DNA content. **a–d** Each histogram represents each cell cycle phase. The bars indicate the average of three replicates and the error bars the standard deviations. 1 mM H_2O_2 and 1% DMSO treatments were included as negative and positive controls for viability, respectively. Statistical difference of the treatments when compared to the solvent (DMSO) are indicated as follows: $*P < 0.05$, $**P < 0.01$, and

Pyr-1 increases *hmox-1* and *noxa* gene and protein expression in HL-60 cells

It has been previously reported that bortezomib, the first FDA-approved proteasome inhibitor used as an anti-cancer drug 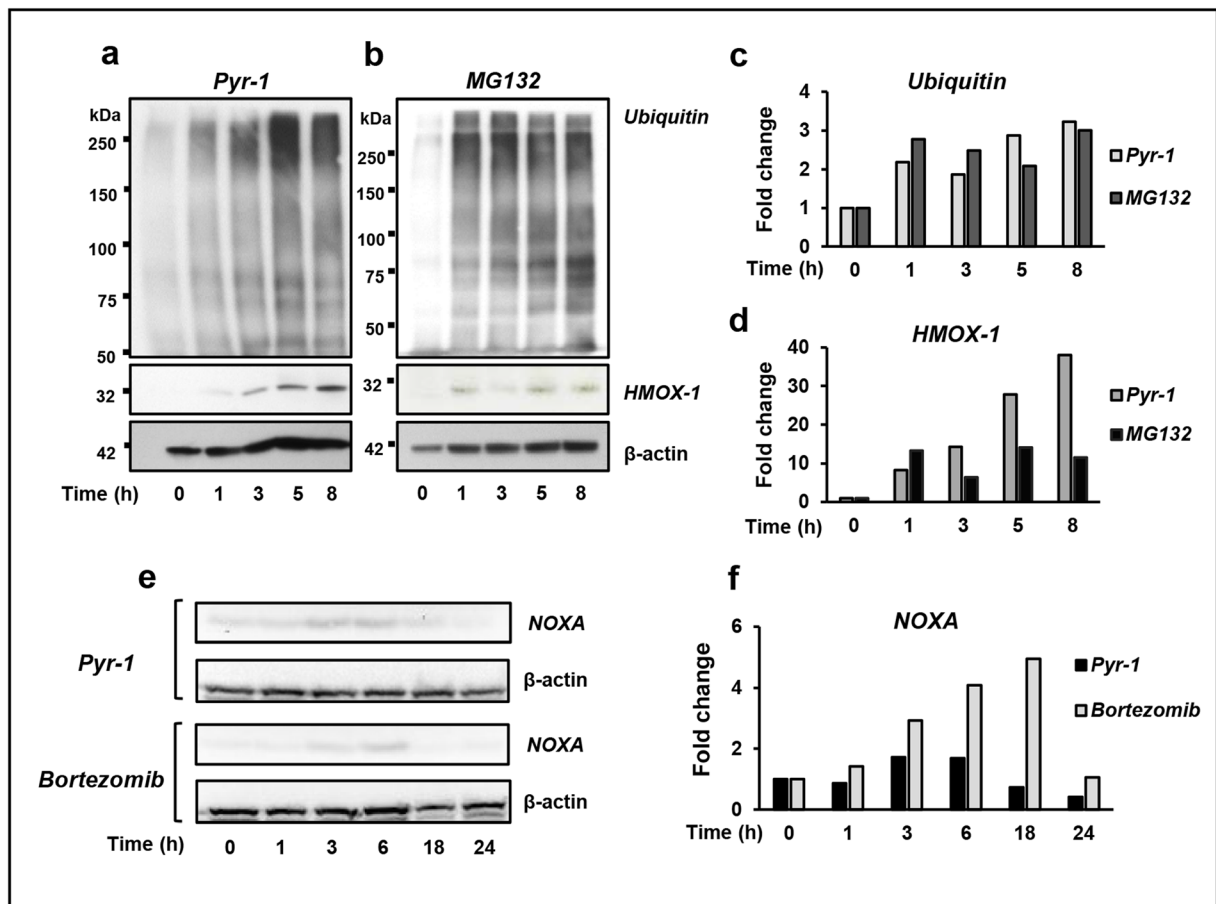for myeloma and solid tumors (Dou and Zonder 2014; Perez-Galan et al. 2006), generates ROS leading to mitochondrial depolarization and apoptosis (Fribley et al. 2004; Ling et al. 2003a; Perez-Galan et al. 2006). At the transcriptional and protein level, bortezomib induces the expression of oxidative stress-related genes such as *hmox-1*, *noxa*, *phox/p67*, and

Fig. 5 Pyr-1 exposure results in poly-ubiquitinated protein accumulation and *hmox-1* and *noxa* protein expression in HL-60 cells. **a**, **b** Ubiquitin and *hmox-1* antibody responses are depicted. Cell lysates were collected at different incubation times with Pyr-1 (0.8 μM) and MG132 (5 μM). β-actin was used as a loading control. **c**, **d** Densitometric analyses of ubiquitin and *hmox-1* protein bands are shown. Bars represent the fold change response of each band per incubation time. Data were normalized using β-actin loading control bands. **e** *Noxa* protein expression is shown in cells treated with Pyr-1 and bortezomib at different exposure times. **f** *Noxa* band signals were quantified by densitrometric analysis and normalized to β-actin. Data is representative of one experiment

many others (Brnjic et al. 2014; Perez-Galan et al. 2006; Qin et al. 2005). Given our previous findings that Pyr-1 acts as a proteasome inhibitor, we sought to explore if Pyr-1 promotes *hmox-1* and/or PMAIP1 (*noxa*) expression at the transcriptional and protein level. *Hmox-1* and *noxa* (also known as PMAIP1) gene expression were measured by RT-qPCR on HL-60 cells treated for 6 h with Pyr-1 or the positive control bortezomib. A robust increase of *hmox-1* mRNA transcripts of 36-fold was observed on Pyr-1 treatments, whereas, *noxa* gene expression did not change significantly (0.36-fold change; Fig. 6). Bortezomib was included as a positive control, and for both genes tested (*hmox-1* and *noxa*), the mRNA transcript levels were augmented, 42- and 5-fold,

respectively (Fig. 6). Values were normalized to the GADPH housekeeping gene. RTq-PCR data was confirmed by Western blotting in HL-60 cells treated with Pyr-1, bortezomib, and MG132 for different incubation times as compared to untreated cells. As shown in Fig. 5a, *hmox-1* protein levels increase in a time-dependent manner after 1-h exposure to Pyr-1. Although an induction of *noxa* at the transcriptional level (Fig. 6) was not observed after 6 h of treatment with Pyr-1, a slight increase in protein levels was detected at 3 and 6 h of exposure (Fig. 5e), suggesting that expression of this gene might have been induced earlier on. Densitometric analyses of the bands of interest were performed and are depicted in Fig. 5d, f for *hmox-1* and *noxa*, respectively.
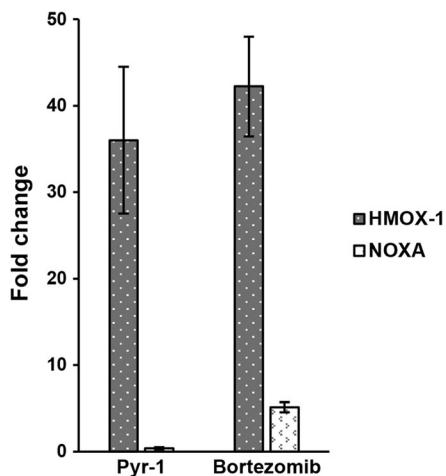
Fig. 6 Pyr-1 strongly activates *hmox-1* gene expression in HL-60-treated cells. After 6 h of Pyr-1 (0.8 μM) and bortezomib (0.06 μM) treatment, RTq-PCR was performed to evaluate mRNA transcript levels of *hmox-1* and *noxa*. Bars represent fold change of gene expression values compared to vehicle controls (PEG/PBS) and normalized to GAPDH housekeeping gene. Error bars indicate standard deviations of three independent experiments, each including three technical replicates

Overall, our results demonstrate that Pyr-1 induces *hmox-1* gene and protein expression as a response to cytotoxic stress.

Discussion

In recent years, pyridazinones have acquired substantial attention due to their extensive biological and pharmacological activities (Akhtar et al. 2016). In this study, we demonstrate that the pyridazinone derivative Pyr-1 exhibits potent cytotoxicity on 22 human cancer cell lines from different tissue origins representing blood hematological cancers (lymphoma, leukemia, and myeloma) and solid tumors (breast, pancreas, prostate, melanoma, ovary, and lung; Table 1). Pyr-1 displayed a favorable selective cytotoxicity against a variety of cancer cells as compared with non-cancerous MCF-10A cells. Pyr-1 exhibited favorable SCIs on the CEM and HL-60 leukemia, on MDA-MB-231 and MDA-MB-468 breast cancer, and A-549 lung cancer cell lines (Table 2). In 2013, *Ovais* et al. reported that three pyridazinone variants exhibited growth inhibitory concentrations (GI$_{50}$) in 36 human cancer cell lines. However, the lethal concentrations (LC$_{50}$) reported for all the tumor cell lines assayed were above 100 μM, indicating low cytotoxicity (Ovais et al. 2013). In addition, these three

pyridazinones were not tested on non-cancerous cells (Ovais et al. 2013). Other studies have also published growth inhibitory concentrations (GI$_{50}$, IC$_{50}$) for other pyridazinone variants, without including non-cancer cell controls, which are important to validate if an experimental compound possesses promising potential as an anti-cancer drug (Elagawany et al. 2013; Shunguang et al. 2014; Xing et al. 2015). Furthermore, these studies were performed by methods that rely on quantifying cell metabolic activity and protein content, such as MTT and SRB assays, respectively, which are indirect approaches to measure cell proliferation or cytotoxicity in cell populations. In contrast, in this study, data was obtained by a direct measurement of cell viability via live-cell imaging through the DNS assay (Lema et al. 2011).

To investigate in greater detail the mechanism used by Pyr-1 to induce cell death, the potential increase in ROS was assessed. It is well known that ROS overproduction damages cell functions, impacting the induction of cell death in many ways such as oxidation of DNA, proteins, and lipids, which in turn affect several signaling pathways throughout the apoptotic pathway (Wu and Bratton 2013). Our data clearly demonstrated that Pyr-1-treated cells induced high levels of ROS (Fig. 2a), suggesting that ROS accumulation is in part responsible for the observed deleterious effects.

The most important source of cellular ROS production is the mitochondria (Suski et al. 2012). Furthermore, there is a very close relationship between the integrity of mitochondrial membrane potential and excessive ROS production (Suski et al. 2012). A consequence of ROS overproduction is mitochondria membrane depolarization, which is an early biochemical event initiating the activation of the intrinsic apoptotic pathway. Our results revealed that Pyr-1 treatment led to mitochondrial depolarization in a dose-dependent manner in HL-60 cells (Fig. 2b).

External environmental stressors, such as the exposure to toxic chemicals, can trigger either apoptosis or necrosis in a cell population. Under homeostasis, phosphatidylserine (PS) is found preferentially in the inner leaflet (cytosolic) of the plasma membrane, but upon cell death induction, it is translocated to the outer leaflet and serves as a sensitive indicator of cells undergoing apoptosis (Leventis and Grinstein 2010). It was previously reported that a pyridazinone (IMB5043) induced apoptosis via PS externalization in the human SMMC-7721 hepatoma cell line (Gong et al. 2018). In addition, increased ROS production resulted in

phosphatidylserine oxidation and facilitated the PS externalization to the plasma membrane in HL-60 cells (Matsura et al. 2002). Pyr-1 ability to induce PS externalization was investigated, and our results indicated that it induces a high level of PS externalization (Fig. 2c), which is a hallmark of apoptosis.

The extrinsic and intrinsic apoptotic pathways converge at the point of execution, which is initiated by the activation of caspase-3. This process causes DNA fragmentation, cytoskeleton degradation, and disintegration of the cell into apoptotic bodies (Elmore 2007; Wu and Bratton 2013). The involvement of caspase-3-induced apoptosis has been previously shown for other pyridazinone derivatives (Gong et al. 2018). Interestingly, other studies have shown that oxidative stress can negatively regulate caspase-3 activation (Huang et al. 2008; Lee and Shacter 2000; Rossig et al. 1999). Our results demonstrated strong caspase-3 activation (Fig. 3) upon Pyr-1 treatment in HL-60 cells, thus proving that Pyr-1 activates the intrinsic apoptotic pathway.

Several apoptotic stimuli provoke cell cycle arrest prior to cell death induction (King and Cidlowski 1998). For instance, the pan-Bcl-2 inhibitor obatoclax, which is active in various cancer cell lines, causes S-G2 arrest, leading to apoptosis (Bates and Lewis 2006). In addition, a compound comprising pyridazinone and thiophene moieties was recently reported to induce apoptosis by arresting the cell cycle in the G2/M-phase (Gong et al. 2018). In the present study, the effects of Pyr-1 treatment on cell cycle progression were investigated. Data demonstrated an increase in the sub-G0-G1 phase, representing the cell subpopulation experiencing DNA fragmentation, concomitant with a decrease in the G0/G1 and G2/M phases (Fig. 4). These findings indicate that Pyr-1 is able to induce DNA fragmentation and also alter the normal cell cycle progression in HL-60 cells.

The most important non-lysosomal pathway in eukaryotic cells, by which proteins are degraded, is the ubiquitin-proteasome system. Through this pathway, target proteins are ubiquitinated and recognized by the 26 S proteasome to be subsequently degraded. Dysfunction of this system has been associated with different diseases, including cancer (Almond and Cohen 2002; Dou and Zonder 2014; Ling et al. 2003a; Perez-Galan et al. 2006). Some reports have associated ROS accumulation to proteasome inhibition and apoptosis induction (Brnjic et al. 2014; Ling et al. 2003b; Perez-Galan et al. 2006). To further elucidate the mechanism by

which Pyr-1 induces cytotoxicity, we evaluated the capacity of Pyr-1 to accumulate poly-ubiquitinated proteins. Data presented in Fig. 5 revealed that Pyr-1 causes poly-ubiquitinated protein accumulation in a similar fashion as the positive control MG132 (Guo and Peng 2013), indicating that proteasome function was impaired.

In a recent publication from our group, transcriptome analyses revealed that two newly discovered proteasome inhibitors induced overexpression of several genes on HL-60 cells with *hmox-1* demonstrating the highest up-regulation of the genes affected by this treatment; and thus *hmox 1* expression was also examined in Pyr-1-treated cells (Contreras et al. 2018). In addition, *noxa*, which is a pro-apoptotic gene, was also previously found to be upregulated by proteasome inhibition (Contreras et al. 2018). Since *noxa* expression promotes cell death, its expression was also examined after Pyr-1-treatment. Moreover, in 2005, a study reported that proteasome inhibitors, such as bortezomib, MG-132, and lactacystin, trigger apoptosis through the induction of *noxa* pro-apoptotic gene and protein in melanoma and myeloma cell lines (Qin et al. 2005). In addition, bortezomib-treated cells showed an excessive generation of ROS and strong induction of *hmox-1* gene/protein expression in colon cancer cells (Brnjic et al. 2014). To evaluate the possibility that Pyr-1 behaves like a proteasome inhibitor, *noxa* and *hmox-1* mRNA transcripts and their protein expression levels were measured in Pyr-1-treated HL-60 cells. Interestingly, a robust increase in *hmox-1* mRNA transcripts and its protein levels was detected after several hours of exposure to Pyr-1 (Figs. 5a and 6). Conversely, *noxa* protein levels from Pyr-1-treated cells were not significantly affected after 3 h of exposure and a very small increase of *noxa* mRNA transcripts was detected (0.36-fold; Fig. 6). Our results suggest that *hmox-1* overexpression triggered by Pyr-1 is likely in response to ROS damage as previously reported (Nath et al. 1992), and also potentially due to proteotoxic stress generated upon proteasome inhibition. The lack of significant *noxa* induction indicates that the mechanism of apoptosis induction by Pyr-1 appears to be different that the mechanism induced by bortezomib, MG132, and lactacystin proteasome inhibitors (Qin et al. 2005).

In summary, Pyr-1 is a novel pyridazinone derivative that has effective anti-cancer activity at nanomolar and low micromolar concentrations on 22 human cancer cell lines. Moreover, Pyr-1

displayed an advantageous selective cytotoxicity on a few leukemia, breast, and lung cancer cell lines. This study further demonstrates that Pyr-1 induces the intrinsic apoptosis pathway as it causes ROS accumulation, mitochondrial depolarization, phosphatidylserine externalization, caspase-3 activation, and alteration of cell cycle progression in acute promyelocytic leukemia. In addition, we report that Pyr-1 activates *hmox-1* gene/protein expression and causes the accumulation of poly-ubiquitinated proteins due to an apparent failure in the ubiquitin-proteasome system. Thus, we conclude that Pyr-1 induces apoptosis via the intrinsic pathway, prompted by ROS accumulation and proteasome inhibition. Pyr-1 could potentially offer a new alternative as an anti-leukemic therapeutic drug, possibly to avoid drug resistance and negative side effects, which can limit the impact and effectiveness of current anti-leukemic drugs. In preliminary studies, Pyr-1 was tested in one mouse at a relatively high concentration of 160 mg/kg given every other day for 6 days (three intraperitoneal doses) and we did not observe any negative side effects (loss of weight, ruffled fur, lethargy, etc). Future work will involve testing Pyr-1 in xenograft models of immunodeficient mice (SCID) bearing human breast tumors (MDA-MB-231) or leukemia (HL-60) to determine its potential for use in cancer-afflicted humans in clinical trials.

References

Akhtar W, Shaquiquzzaman M, Akhter M, Verma G, Khan MF, Alam MM. The therapeutic journey of pyridazinone. Eur J Med Chem. 2016;123:256–81.

Al-Lazikani B, Banerji U, Workman P. Combinatorial drug therapy for cancer in the post-genomic era. Nat Biotechnol. 2012;30:679–92.

Almond JB, Cohen GM. The proteasome: a novel target for cancer chemotherapy. Leukemia. 2002;16:433–43.

American Cancer Society. 2017. Cancer Facts & Figures 2017.

Asif M. A mini review on biological activities of pyridazinone derivatives as antiulcer, antisecretory, antihistamine and particularly against histamine H3R. Mini-Rev Med Chem. 2015;14:1093–103.

Bates DJ, Lewis LD. Manipulating the apoptotic pathway: potential therapeutics for cancer patients. Br J Clin Pharmacol. 2006;76:381–95.

Brnjic S, Mazurkiewicz M, Fryknas M, Sun C, Zhang X, Larsson R, et al. Induction of tumor cell apoptosis by a proteasome deubiquitinase inhibitor is associated with oxidative stress. Antioxid Redox Signal. 2014;21:2271–85.

Chen L, Brewer MD, Guo L, Wang R, Jiang P, Yang X. Enhanced degradation of misfolded proteins promotes tumorigenesis. Cell Rep. 2017;18:3143–54.

Contreras L, Calderon RI, Varela-Ramirez A, Zhang HY, Quan Y, Das U, et al. Induction of apoptosis via proteasome inhibition in leukemia/lymphoma cells by two potent piperidones. Cell Oncol. 2018;41(6):623–36.

Costas T, Costas-Lago MC, Vila N, Besada P, Cano E, Teran C. New platelet aggregation inhibitors based on pyridazinone moiety. Eur J Med Chem. 2015;94:113–22.

D'Arcy P, Brnjic S, Olofsson MH, Fryknas M, Lindsten K, De Cesare M, et al. Inhibition of proteasome deubiquitinating activity as a new cancer therapy. Nat Med. 2011;17:1636–40.

Dorsch D, Schadt O, Stieber F, Meyring M, Gradler U, Bladt F, et al. Identification and optimization of pyridazinones as potent and selective c-met kinase inhibitors. Bioorg Med Chem Lett. 2015;25:1597–602.

Dou QP, Zonder JA. Overview of proteasome inhibitor-based anti-cancer therapies: perspective on Bortezomib and second generation proteasome inhibitors versus future generation inhibitors of ubiquitin proteasome system. Curr Cancer Drug Targets. 2014;14:517–36.

Elagawany M, Ibrahim MA, Ali Ahmed HE, El-Etrawy AS, Ghiaty A, Abdel-Samii ZK, et al. Design, synthesis, and molecular modelling of pyridazinone and phthalazinone derivatives as protein kinases inhibitors. Bioorg Med Chem Lett. 2013;23:2007–13.

Elmore S. Apoptosis: a review of programmed cell death. Toxicol Pathol. 2007;35:495–516.

Eruslanov E, Kusmartsev S. Identification of ROS using oxidized DCFDA and flow-cytometry. Methods Mol Biol. 2010;594:57–72.

Faidallah HM, Rostom SAF, Basaif SA, Makki MST, Khan KA. Synthesis and biological evaluation of some novel urea and thiourea derivatives of isoxazolo[4,5-d]pyridazine and structurally related thiazolo[4,5-d]pyridazine as anti-microbial agents. Arch Pharm Res. 2013;36:1354–68.

Fribley A, Zeng Q, Wang CY. Proteasome inhibitor PS-341 induces apoptosis through induction of endoplasmic reticulum stress-reactive oxygen species in head and neck squamous cell carcinoma cells. Mol Cell Biol. 2004;24:9695–704.

Fulda S, Debatin KM. Extrinsic versus intrinsic apoptosis pathways in anticancer chemotherapy. Oncogene. 2006;25:4798–811.

Gong J, Zheng Y, Wang Y, Sheng W, Li Y, Liu X, et al. A new compound of thiophenylated pyridazinone IMB5043 showing potent antitumor efficacy through ATM-Chk2 pathway. PLoS One. 2018;13:e0191984.

Guo N, Peng Z. MG132, a proteasome inhibitor, induces apoptosis in tumor cells. Asia Pac J Clin Oncol. 2013;9:6–11.

Hanahan D, Weinberg RA. The hallmarks of cancer. Cell. 2000;100:57–70.

Hanahan D, Weinberg RA. Hallmarks of cancer: the next generation. Cell. 2011;144:646–74.

Huang Z, Pinto JT, Deng H, Richie JP Jr. Inhibition of caspase-3 activity and activation by protein glutathionylation. Biochem Pharmacol. 2008;75:2234–44.

Invitrogen. Reactive oxygen species (ROS) detection reagents. In: Eugene, OR. Invitrogen: Molecular Probes; 2006.

Jacomini AP, Silva MJV, Silva RGM, Goncalves DS, Volpato H, Basso EA, et al. Synthesis and evaluation against Leishmania amazonensis of novel pyrazolo[3,4-d]pyridazinone-N-acylhydrazone-(bi)thiophene hybrids. Eur J Med Chem. 2016;124:340–9.

Jin X, Wang Y, Tan L, He Y, Peng J, Hai L, et al. An efficient injectable formulation with block copolymer micelles for hydrophobic antitumor candidate-pyridazinone derivatives. Nanomedicine (London). 2015;10:2153–65.

King KL, Cidlowski JA. Cell cycle regulation and apoptosis. Annu Rev Physiol. 1998;60:601–14.

Lee YJ, Shacter E. Hydrogen peroxide inhibits activation, not activity, of cellular caspase-3 in vivo. Free Radic Biol Med. 2000;29:684–92.

Lema C, Varela-Ramirez A, Aguilera RJ. Differential nuclear staining assay for high-throughput screening to identify cytotoxic compounds. Curr Cell Biochem. 2011;1:1–14.

Leonard JP, Furman RR, Coleman M. Proteasome inhibition with bortezomib: a new therapeutic strategy for non-Hodgkin's lymphoma. Int J Cancer. 2006;119:971–9.

Leventis PA, Grinstein S. The distribution and function of phosphatidylserine in cellular membranes. Annu Rev Biophys. 2010;39:407–27.

Li B, Dou QP. Bax degradation by the ubiquitin/proteasome-dependent pathway: involvement in tumor survival and progression. Proc Natl Acad Sci. 2000;97:3850–5.

Li K, Schurig-Briccio LA, Feng X, Upadhyay A, Pujari V, Lechartier B, et al. Multitarget drug discovery for tuberculosis and other infectious diseases. J Med Chem. 2014;57:3126–39.

Ling HE, Liebes L, Zou Y, Perez-Soler R. Reactive oxygen species generation and mitochondrial dysfunction in the apoptotic response to Bortezomib, a novel proteasome inhibitor, in human H460 non-small cell lung Cancer cells. J Biol Chem. 2003a;278:33714–23.

Ling YH, Liebes L, Zou Y, Perez-Soler R. Reactive oxygen species generation and mitochondrial dysfunction in the apoptotic response to Bortezomib, a novel proteasome inhibitor, in human H460 non-small cell lung cancer cells. J Biol Chem. 2003b;278:33714–23.

Liu Y, Jin S, Peng X, Lu D, Zeng L, Sun Y, et al. Pyridazinone derivatives displaying highly potent and selective inhibitory activities against c-met tyrosine kinase. Eur J Med Chem. 2016;108:322–33.

Loda M, Cukor B, Tam SW, Lavin P, Fiorentino M, Draetta GF, et al. Increased proteasome-dependent degradation of the cyclin-dependent kinase inhibitor p27 in aggressive colorectal carcinomas. Nat Med. 1997;3:231–4.

Matsura T, Serinkan BF, Jiang J, Kagan VE. Phosphatidylserine peroxidation/externalization during staurosporine-induced apoptosis in HL-60 cells. FEBS Lett. 2002;524:25–30.

Mogilski S, Kubacka M, Redzicka A, Kazek G, Dudek M, Malinka W, et al. Antinociceptive, anti-inflammatory and smooth muscle relaxant activities of the pyrrolo[3,4-d]pyridazinone derivatives: possible mechanisms of action. Pharmacol Biochem Behav. 2015;133:99–110.

Munoz R, Man S, Shaked Y, Lee CR, Wong J, Francia G, et al. Highly efficacious nontoxic preclinical treatment for advanced metastatic breast cancer using combination oral UFTCyclophosphamide metronomic chemotherapy. Cancer Res. 2006;66:3386–91.

Nastiuk KL, Krolewski JJ. Opportunities and challenges in combination gene cancer therapy. Adv Drug Deliv Rev. 2016;98:35–40.

Nath KA, Balla G, Vercellotti G. Induction of heme oxygenase is a rapid, protective response in rhabdomyolysis in the rat. J Clin Invest. 1992;90:267–70.

Naujokat C, Hoffmann S. Role and function of the 26S proteasome in proliferation and apoptosis. Lab Investig. 2002;82:965–80.

Ovais S, Javed K, Yaseen S, Bashir R, Rathore P, Yaseen R, et al. Synthesis, antiproliferative and anti-inflammatory activities of some novel 6-aryl-2-(p-(methanesulfonyl)phenyl)-4,5-dihydropyridazi3(2H)-ones. Eur J Med Chem. 2013;67:352–8.

Perez-Galan P, Roue G, Villamor N, Montserrat E, Campo E, Colomer D. The proteasome inhibitor bortezomib induces apoptosis in mantle-cell lymphoma through generation of ROS and Noxa activation independent of p53 status. Blood. 2006;107:257–64.

Qin JZ, Ziffra J, Stennett L, Bodner B, Bonish BK, Chaturvedi V, et al. Proteasome inhibitors trigger NOXA-mediated apoptosis in melanoma and myeloma cells. Cancer Res. 2005;65:6282–93.

Ramaswami R, Harding V, Newsom-Davis T. Novel cancer therapies: treatments driven by tumour biology. Postgrad Med J. 2013;89:652–8.

Rathish IG, Javed K, Bano S, Ahmad S, Alam MS, Pillai KK. Synthesis and blood glucose lowering effect of novel pyridazinone substituted benzenesulfonylurea derivatives. Eur J Med Chem. 2009;44:2673–8.

Reece DE, Hegenbart U, Sanchorawala V, Merlini G, Palladini G, Bladé J, et al. Efficacy and safety of once-weekly and twice-weekly bortezomib in patients with relapsed systemic AL amyloidosis: results of a phase 1/2 study. Blood. 2011;118:865–73.

Robles-Escajeda E, Das U, Ortega NM, Parra K, Francia G, Dimmock JR, et al. A novel curcumin-like dienone induces

apoptosis in triple-negative breast cancer cells. Cell Oncol. 2016;39:265–77.

Robles-Escajeda E, Lerma C, Nyakeriga AM, Ross JA, Kirken RA, Aguilera RJ, et al. Searching in Mother Nature for Anti-Cancer Activity: AntiProliferative and Pro-Apoptotic Effect Elicited by Green Barley on Leukemia/Lymphoma Cells. PLoS One. 2013;8:e73508.

Rossig L, Fichtlscherer B, Breitschopf K, Haendeler J, Zeiher AM, Mulsch A, et al. Nitric oxide inhibits caspase- 3 by S-nitrosation in vivo. J Biol Chem. 1999;274:6823–6.

Saini M, Mehta DK, Das R, Saini G. Recent advances in anti-inflammatory potential of Pyridazinone derivatives. Mini-Rev Med Chem. 2016;16:996–1012.

Santiago-Vazquez Y, Das U, Varela-Ramirez A, Baca ST, Ayala-Marin Y, Lema C, et al. Tumor-selective cytotoxicity of a novel pentadiene analogue on human leukemia/ lymphoma cells. Clin Cancer Drugs. 2016;3:138–46.

Schmittgen TD, Livak KJ. Analyzing real-time PCR data by the comparative CT method. Nat Protoc. 2008;3:1101–8.

Shunguang Z, Huimin L, Chao H, Yanan D, Mingyan J, Lixiang R, et al. Design, synthesis and structureeactivity relationships of novel 4-phenoxyquinoline derivatives containing pyridazinone moiety as potential antitumor agents. Eur J Med Chem. 2014;83:581–93.

Suski J, Lebiedzinska M, Bonora M, Pinton P, Duszynski J, Wieckowski MR. Relation between mitochondrial membrane potential and ROS formation. Methods Mol Biol. 2018;1782:357–81.

Suski JM, Lebiedzinska M, Bonora M, Pinton P, Duszynski J, Wieckowski MR. Relation between mitochondrial membrane potential and ROS formation. Methods Mol Biol. 2012;810:183–205.

Tewari KM, Dhaneshwar SS. Inhibitors of apoptosis proteins (IAPs): clinical significance in Cancer treatment research. J Can Res Updates. 2012;1:212–20.

Torres-Roca JF, Lecoeur H, Amatore C, Gougeon ML. The early intracellular production of a reactive oxygen intermediate mediates apoptosis in dexamethasone-treated thymocytes. Cell Death Differ. 1995;2:309–19.

Varela-Ramirez A, Costanzo M, Carrasco YP, Pannell KH, Aguilera RJ. Cytotoxic effects of two organotin compounds and their mode of inflicting cell death on four mammalian cancer cells. Cell Biol Toxicol. 2011;27:159–68.

Wada N, Kawano Y, Fujiwara S, Kikukawa Y, Okuno Y, Tasaki M, et al. Shikonin, dually functions as a proteasome inhibitor and a necroptosis inducer in multiple myeloma cells. Int J Oncol. 2015;46:963–72.

Wang YJ, Lu D, Xu YB, Xing WQ, Tong XK, Wang GF, et al. A novel pyridazinone derivative inhibits hepatitis B virus replication by inducing genome-free capsid formation. Antimicrob Agents Chemother. 2015;59:7061–72.

WHO. 2018. Cancer. WHO [Online] Available: http://www.who.int/news-room/fact-sheets/detail/cancer [Accessed 7–31-18].

Wu CC, Bratton SB. Regulation of the intrinsic apoptosis pathway by reactive oxygen species. Antioxid Redox Signal. 2013;19:546–58.

Xing W, Ai J, Jin S, Shi Z, Peng X, Wang L, et al. Enhancing the cellular anti-proliferation activity of pyridazinones as cmet inhibitors using docking analysis. Eur J Med Chem. 2015;95:302–12.

Zhang J, Wu P, Hu Y. Clinical and marketed proteasome inhibitors for Cancer treatment. Curr Med Chem. 2013;20:2537–51.

Zhou S, Liao H, He C, Dou Y, Jiang M, Ren L, et al. Design, synthesis and structure-activity relationships of novel 4-phenoxyquinoline derivatives containing pyridazinone moiety as potential antitumor agents. Eur J Med Chem. 2014;83:581–93.